

## Research Paper

**Cite this article:** Ghazali AN, Sazid M (2022). Design of multiple transmission zeros-enabled compact broadband BPFs based on microstrip-to-CPW transition technology. *International Journal of Microwave and Wireless Technologies* **14**, 546–552. <https://doi.org/10.1017/S1759078721000763>

Received: 15 November 2020  
Revised: 26 April 2021  
Accepted: 26 April 2021  
First published online: 19 May 2021

### Keywords:

Bandpass filter (BPF); folded split ring resonator (FSRR); microstrip-to-CPW transition; multiple mode resonator (MMR); ultra-wideband (UWB)

### Author for correspondence:

Abu Nasar Ghazali,  
E-mails: [anghazali@gmail.com](mailto:anghazali@gmail.com),  
[abu.ghazalifet@kiit.ac.in](mailto:abu.ghazalifet@kiit.ac.in)

© The Author(s), 2021. Published by Cambridge University Press in association with the European Microwave Association

**CAMBRIDGE**  
UNIVERSITY PRESS

# Design of multiple transmission zeros-enabled compact broadband BPFs based on microstrip-to-CPW transition technology

Abu Nasar Ghazali<sup>1</sup>  and Mohd Sazid<sup>2</sup>

<sup>1</sup>School of Electronics Engineering, Kalinga Institute of Industrial Technology (KIIT), Deemed University, Bhubaneswar 751024, Odisha, India and <sup>2</sup>Department of Electronics and Communication Engineering, Delhi Technological University, Delhi 110042, India

## Abstract

In this paper, we present a miniaturized ultra-wideband (UWB) bandpass filter (BPF) with multiple transmission zeros (TZs), which is based on transition technology of microstrip with short-circuited coplanar waveguide (CPW). The ground plane of the BPF contains a multiple mode resonator (MMR)-based CPW which is capacitively linked through the dielectric to two open-circuited microstrip lines on the top. The MMR is initially designed to allocate its lowest three resonant modes quasi-equally inside the designated UWB spectrum (3.1–10.6 GHz). This is followed by optimization of microstrip lines to provide a good broadband response possessing minimum insertion loss, two TZs at the lower and upper passband edges that improve selectivity and a wide stopband with appreciable attenuation. Later, multiple-folded split ring resonators are coupled to the BPF to inject dual passband TZs. The predicted theory in simulation is verified against measured result and is found to be in good agreement. The prototype covers a substrate area of only  $14.6 \times 9.2 \text{ mm}^2$ .

## Introduction

Research on design and development of passive ultra-wideband (UWB) components has taken an exponential leap since the allocation of 3.1–10.6 GHz spectrum by the Federal Communications Commission (FCC) for indoor communications [1]. One such essential component of UWB systems is an UWB bandpass filter (BPF), which was designed using different principles [2–8]. An initial filter designed in this respect consisted of a microstrip line mounted on a composite lossy substrate to realize attenuation at high frequencies [2], whereas the basic idea of cascading high pass filters with low pass filters to develop an UWB-BPF was used in [3]. Perhaps, the most convenient method used in designing UWB filters was using a multiple mode resonator (MMR) which provides the flexibility of adjusting the bandwidth using its inherent resonant modes [4, 5]. Another excellent method of UWB filter construction is using the transition technology of microstrip-to-coplanar waveguide (CPW) transition [6, 7]. The ground plane consists of CPW-based open-circuited or short-circuited MMR which is designed to place its resonant modes within the UWB passband and then the optimized coupling of the transition generates a smooth passband.

Recently, the UWB spectrum has got crowded due to the dense population of several RF sources such as WLAN, C band, RFID, X band, etc. These RF sources many a times create interference issues in the short range environment wherein UWB systems operate. In order to check such unwanted interferences UWB-BPFs are often embedded with bandstop filters, which utilize their transmission zeros (TZs) to circumvent interferences. The most common method of developing TZs is by the defected ground structures (DGSs) [8] or slots in microstrips [9, 10]. Two complementary split ring resonator (CSRR)-shaped DGS were used to develop dual notches in [8], whereas slots in microstrip on the top in the form of spurlines [9] and CSRR [10] generated dual TZs in the passband. A very popular method of notch generation is with the use of stepped impedance resonator (SIR) along the microstrip [11–16]. The SIR in its original form [11–13], or in the form of simplified composite right/left-handed resonator [14], E-shaped resonator [15], or electromagnetic (EM) band gap structures [13] has dual resonance properties which help in placing two notches at points of interest in the passband. Folded microstrip lines utilize the principle of wave cancellation for generation of two TZs in [17]. Other dual-notched band structures reported used the combination of any two of the abovementioned principles [18–20]. Folded lines combined with slots (stubs) in microstrips were utilized for dual stopband generation in [18], whereas DGS with multiple SRRs [19], and DMS with SIR [20] placed two TZs in the passband. A recently published study developed dual notches using folded SRRs [21]. The authors in [22, 23] report work on tunable passband notches. However, most of the structures mentioned above possess several drawbacks in the form of absence of TZs [8, 11–20] which leads to poor selectivity [11, 13–16, 18], poor

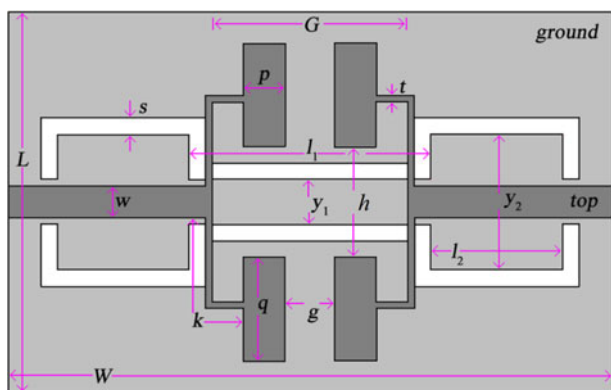


**Fig. 1.** Microstrip-to-CPW transition-based proposed UWB filter. Dark shade conductor and white shade etched part. All dimensions are in mm.

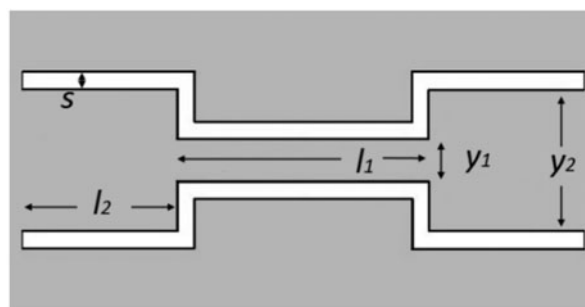
return/insertion loss [9, 11–14, 16–18], large size [8, 10–12, 14, 16, 18, 20, 21], and complex geometry due to presence of vias [11–16, 18, 20] or limitation in fabrication caused by minimum dimension [10, 17].

In this paper, we report a miniaturized dual band-notched UWB-BPF which overcomes the abovementioned shortcomings. The proposed BPF is developed on the technology of microstrip-to-CPW transition. Here, microstrip lines are oriented back-to-back on the top and electromagnetically coupled to the short-circuited MMR-based CPW in the ground (Fig. 1). Initially, the short-circuited MMR is manipulated in dimensions to situate its first three resonant modes near the lower, central and upper end of requisite UWB spectrum. Later, microstrip lines on top are tuned accordingly in dimensions so as to ensure a tight coupling of the transition thereby generating the specified UWB spectrum. This frequency characteristic contains multiple TZs, minimum insertion loss, high return loss, wide stopband, and flat group delay. Finally, multiple-folded split ring resonators (FSRRs) are embedded into the basic BPF to develop two TZs so as to cut out WLAN and X band frequencies from the passband. Commercial full-wave EM software IE3D was used to optimize the structure on the RT/Duriod 6010 substrate with  $\epsilon_r = 10.8$ , height 0.635 mm, and loss tangent 0.0023. The following sections deal with the design and implementation of the proposed UWB-BPF. The current study is a hybrid design mix of [4] and [6]. The BPF in the current study is based on the microstrip-to-CPW transition technology, similar to [6]; however, it utilizes a short-circuited MMR-based CPW (similar to [4]) in the ground (unlike [6] which has uniform resonator-based short-circuited CPW in the ground). Also, in [4], the MMR-based CPW and its driving resonators are on the same surface at the top, whereas, in our BPF, the MMR-based CPW and its driving resonators (microstrip lines) are on opposite sides of the substrate. The present BPF possesses TZs at either passband edges which brings about good selectivity, unlike [4, 6]. Structures of [4, 6] display narrow stopbands, whereas the proposed BPF has wider stopband. Also, the proposed BPF is much compact in size compared to [4, 6].

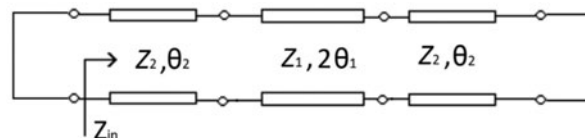
### Proposed UWB filter

#### CPW-based short-circuited MMR

The ground plane consists of a short-circuited CPW with MMR etched in it. The MMR has two similar low-impedance (wide) sections on either side of one high-impedance (narrow) central section. The geometry and equivalent transmission line model



(a)



(b)

**Fig. 2.** (a) Geometry of the MMR-based CPW. (b) Equivalent transmission line model.

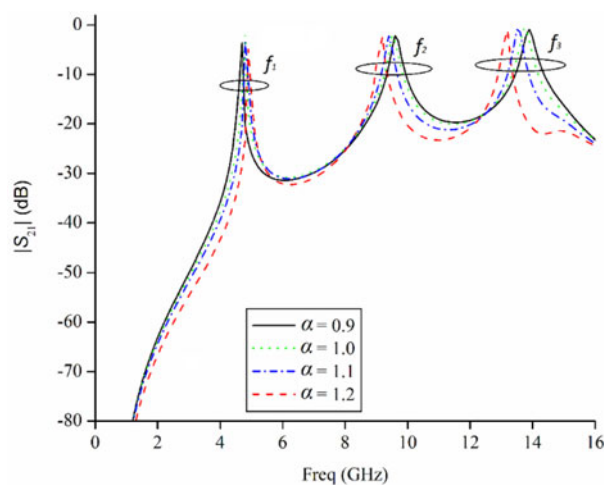


**Fig. 3.** Weak coupling response for a variable impedance ratio.

of the CPW are depicted in Figs 2(a) and 2(b). Our analysis overlooks the two CPW-step discontinuities at the end since their effect is minimal on the UWB characteristics [4]. To utilize the MMR characteristics for design of UWB-BPF, the resonant condition of all the modes must be established. In view of this, the input impedance at the left short-end ( $Z_{in}$ ), looking into the right is derived and depicted in equation (1):

$$Z_{in} = jZ_2 \frac{2(\alpha \tan \theta_1 + \tan \theta_2)(\alpha - \tan \theta_1 \tan \theta_2)}{\alpha(1 - \tan^2 \theta_1)(1 - \tan^2 \theta_2) - 2(1 + \alpha^2) \tan \theta_1 \tan \theta_2} \quad (1)$$

Here,  $\alpha = Z_1/Z_2$ ,  $Z_1$  is the impedance of the central section, whereas  $Z_2$  is the impedance of the end sections. At the resonance condition,  $Z_{in} = 0$ , and generates some set of equations which upon solving provide  $f_1$ ,  $f_2$ , and  $f_3$ . For the proposed structure, the central section of MMR has dimensions,  $l_1 = 5.835$  mm ( $\approx \lambda_{gCPW1}/4$ ),  $y_1 = 0.982$  mm,  $s = 0.42$  mm, for which  $Z_1 = Z_0$  ( $_{CPW1}$ ) = 51.58  $\Omega$  and  $\theta_1 = 52.15^\circ$ . Similarly, for the end sections

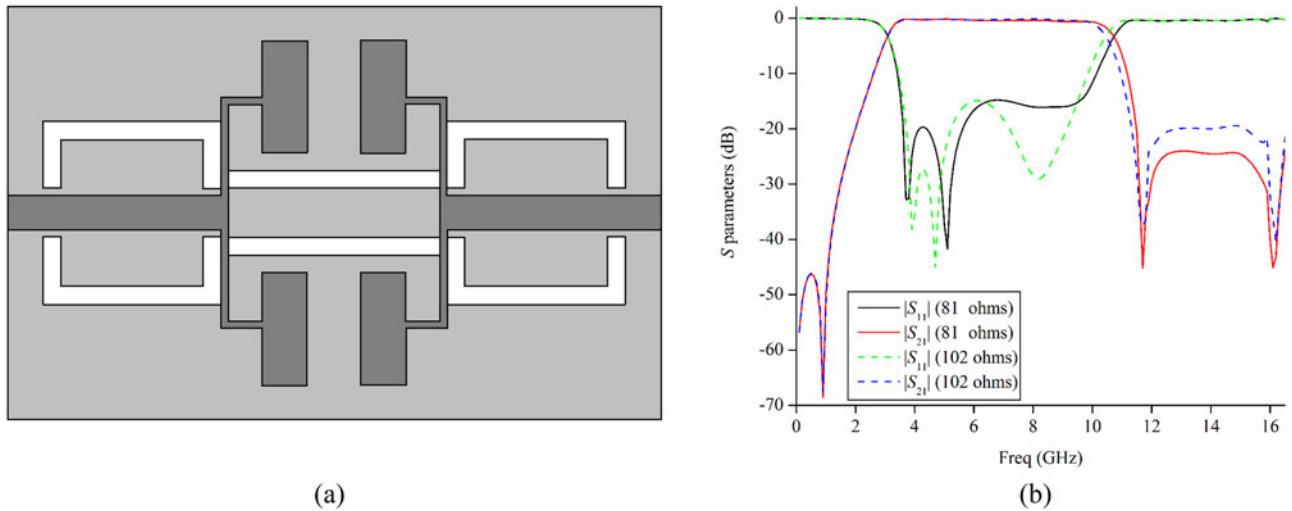


Fig. 4. (a) Architecture of the basic UWB-BPF. (b) Comparative frequency characteristics for variable impedance of CPW.

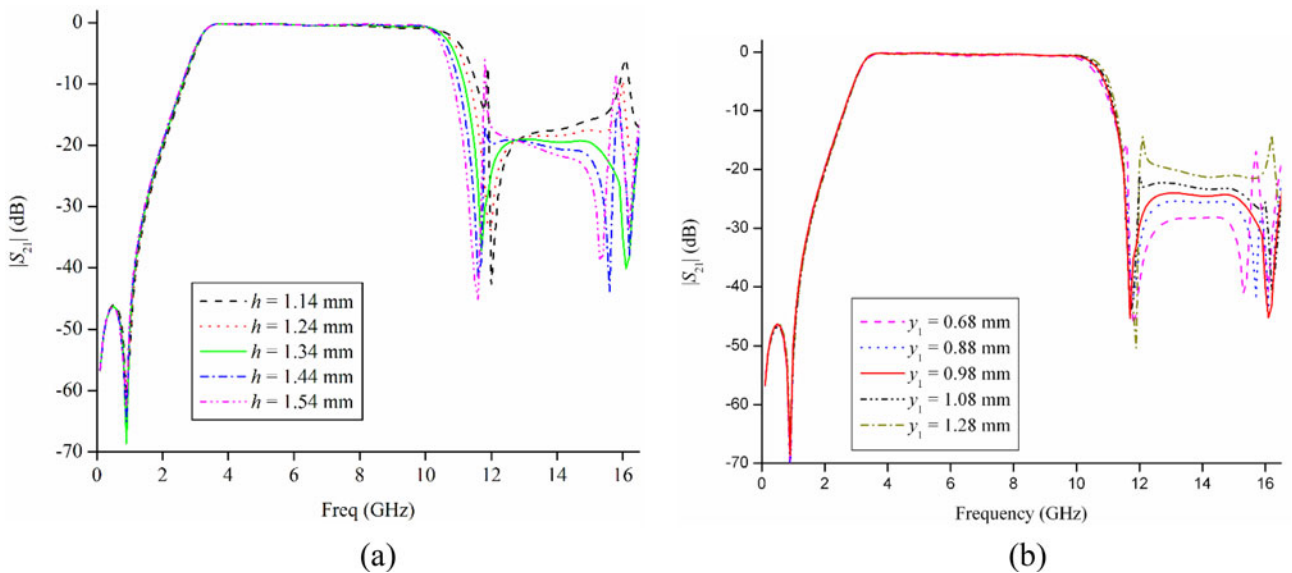


Fig. 5. Variable transmission characteristics for (a)  $h$  and (b)  $y_1$ .

Table 1. Optimized dimensions of the proposed UWB-BPF

Parameters	$L$	$W$	$G$	$l_1$	$l_2$	$y_1$	$y_2$	$h$
Dimension (mm)	14.6	9.2	4.75	5.83	3.185	0.98	3.28	1.34
Parameters	$q$	$g$	$S$	$p$	$t$	$w$	$k$	
Dimension (mm)	2.5	1.2	0.4	1	0.15	0.76	3.115	

of the MMR,  $Z_2 = Z_{0(CPW2)} = 41.4 \Omega$  and  $\theta_2 = 51^\circ$ , corresponding to dimensions,  $l_2 = 3.185 \text{ mm}$  ( $\approx \lambda_{gCPW2}/8$ ),  $y_2 = 3.284 \text{ mm}$ , and  $s = 0.42 \text{ mm}$ . It can be observed from above that the electrical lengths of three sections are approximately,  $\theta_1 \approx \theta_2 \approx \theta$ , and  $\alpha = Z_1/Z_2 = 1.2$ . Hence, the first three resonant frequencies evaluated are:

$$f_1 = (c/2\pi l_1) \tan^{-1} \sqrt{\alpha} \tag{2}$$

$$f_2 = c/4l_1 \tag{3}$$

$$f_3 = (c/2\pi l_1)(\pi - \tan^{-1} \sqrt{\alpha}) \tag{4}$$

The above equations depict that the extreme frequencies ( $f_1, f_3$ ) are mainly affected by the impedance ration, whereas the mid frequency ( $f_2$ ) is a function of length of central section. The weak coupling response of the CPW-based MMR against variable impedance ratio is plotted in Fig. 3 from which can be observed that for reducing  $\alpha$ , the lowest resonant mode ( $f_1$ ) deviates left, whereas the higher ones ( $f_2, f_3$ ) shift right.

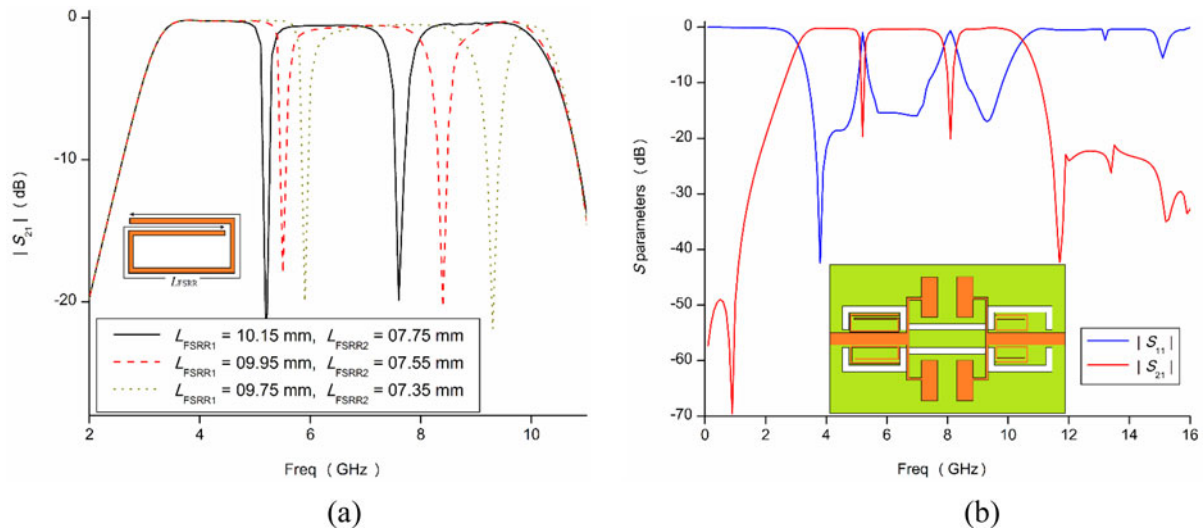


Fig. 6. (a) Variable position of passband TZs for different lengths of the FSRR. (b) Optimized frequency characteristics of the proposed dual-notched UWB-BPF.

**Microstrip-to-CPW transition**

Having modeled the CPW, the objective next becomes optimizing the transition so as to generate the requisite UWB spectrum with good frequency characteristics such as minimum insertion loss and multiple TZs. The transition coupling is of capacitive nature

and maximum coupling at the central UWB frequency (6.85 GHz) can be achieved by matching the characteristic impedances of the microstrip line with that of CPW i.e.  $Z_{0(\text{microstrip})} = 2Z_0(\text{CPW1})$  [6]. In the structure under consideration,  $Z_{0(\text{CPW1})} = 51 \Omega$ , and for  $t = 0.15$  mm,  $Z_{0(\text{microstrip})} = 81 \Omega$ . Ideally  $Z_{0(\text{microstrip})} =$

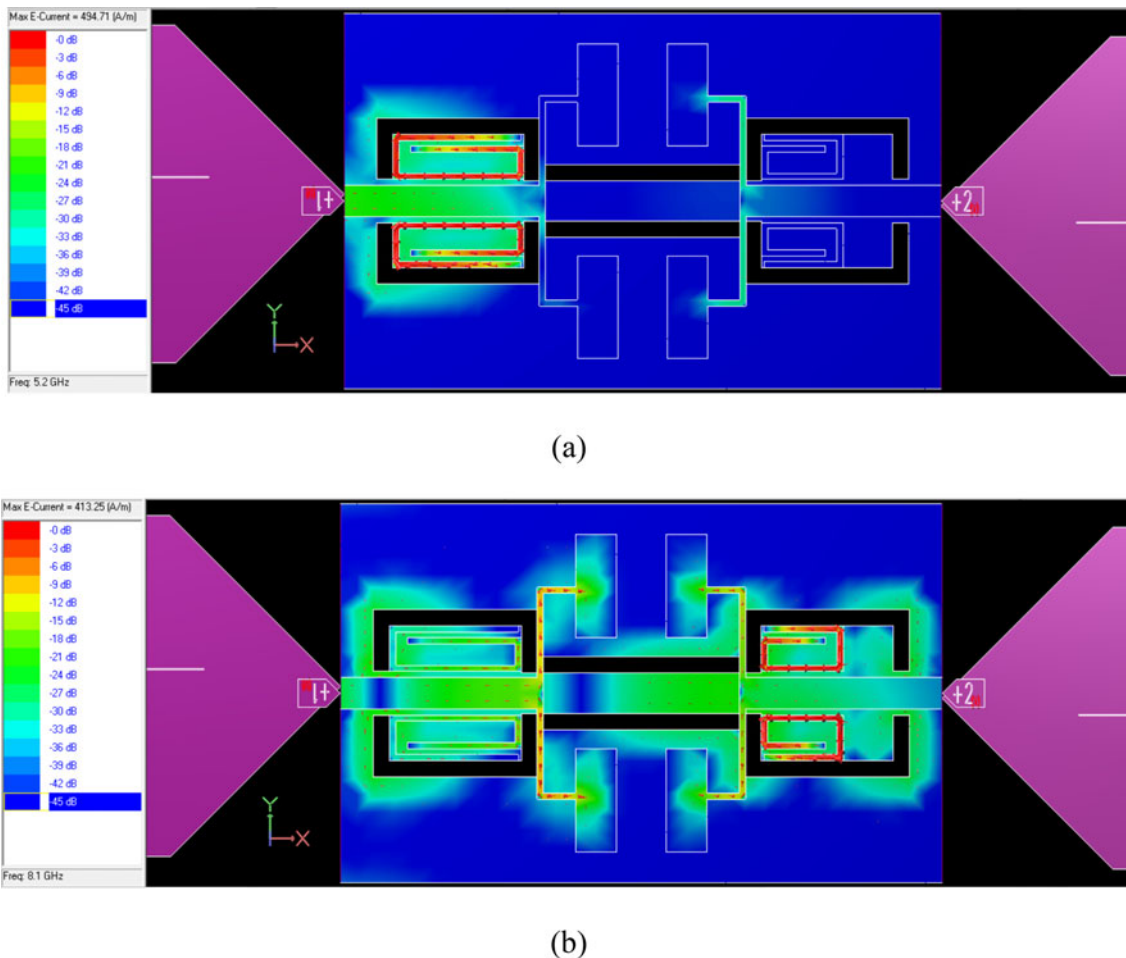


Fig. 7. Current distribution in the BPF at (a) 5.2 GHz and (b) 8.1 GHz.

102  $\Omega$  would have best suited the above relation, however, 81  $\Omega$  is used because it provides wider bandwidth, proper upper TZ and spurious free stopband with a negligible effect on other frequency characteristics as depicted in Fig. 4. Also, for  $Z_{0(\text{microstrip})} = 102 \Omega$ , the thickness of microstrip lines,  $t = 0.12$  mm is little difficult to fabricate. From the simulated response of Fig. 4, it can be observed that the passband extends from 3.05 to 10.7 GHz with return/insertion loss better than 15/0.54 dB. The two TZs at 0.95 and 11.7 GHz provide a sharp roll-off  $>34$  and 48 dB/GHz respectively at lower and upper passband edges. The third TZ at 16 GHz ensures a spurious-free stopband with attenuation  $>25$  dB.

The other parameters can be altered to tune the frequency characteristics of the basic UWB-BPF. For example, Figs 5(a) and 5(b) depict the variation of frequency response for vertical height ( $h$ ) and length of the central section of the CPW,  $y_1$ . It can be observed that variation in vertical separation ( $h$ ) alters the TZs located at the higher passband end and in stopband without affecting the position of lower TZ. The fine tuning of  $y_1$  brings about changes in impedances  $Z_1$  which enhances the passband and stopband characteristics of our proposed structure. Also, the horizontal separation ( $g$ ) controls the position of all three TZs, as well as selectivity at lower and upper passband/stopband edges. For small values of  $g$ , the two roll-offs at passband/stopband edges show increased selectivity but at the cost of reduced stopband width due to the presence of transmission poles (TPs) at around 12 and 15.5 GHz. However, for optimum value of  $g = 1.2$  mm, we get the requisite UWB passband width as well as increased stopband, due to suppression of TPs at 12 and 15.5 GHz respectively. Increasing  $g$  beyond this again brings about a deterioration in frequency response. The optimized dimension of the UWB-BPF is provided in Table 1.

### Implementation of notches across the passband

To the basic UWB-BPF developed above, multiple FSRRs are appended on the top plane close to the feed line. These FSRRs develop notches (TZs) which are placed at frequencies of interest in the passband. The position of notch (TZ) is a function of the FSRR length and given by the formula:

$$f_{\text{notch}} \approx c/4(L_{\text{FSRR}}\sqrt{\epsilon_{\text{eff}}}) \quad (5)$$

Figure 6(a) depicts the tunability range of the FSRR for its variable length. For our design, FSRRs of appropriate lengths are selected to circumvent interferences at 5.2 GHz (WLAN) and 8.1 GHz (X band). The optimized dual-notched band response of the proposed BPF is depicted in Fig. 6(b), from which it can be observed that passband has a frequency spread from 3 to 10.65 GHz. Multiple TZs are observed, two at the passband edges (0.9 and 11.8 GHz) and two within it (5.2 and 8.1 GHz). The TZs have attenuation of at least 20 dB. The passband insertion/return loss is better than 0.32/15 dB (except for the dual notches). The stopband has an attenuation of 22 dB until 16 GHz. At their respective frequency of resonance, the respective FSRRs are tightly coupled to the BPF, as evident from their current distributions in Fig. 7. The FSRRs have high current concentration at the dual notch frequencies of 5.2 and 8.1 GHz, respectively, which represents their affect in generating those TZs

### Experimental verification

To verify the predicted simulated performance, the structure is fabricated and its response measured using an Agilent Vector Network

Analyzer N5230A. Figure 8(a) shows the measured passband frequency characteristics which extend from 3.06 to 10.73 GHz with insertion loss  $<1.4$  dB and return loss  $>13$  dB. Most of the structures do not report insertion loss due to their poor frequency characteristics [9, 13–16], whereas few [18, 21] have very high insertion loss. Stopband observed is spurious free until 16 GHz with attenuation  $>22.6$  dB. The dual passband notches are located at 5.28 and 8 GHz with attenuation better than 19 dB. From Fig. 8(b), it is observed that the measured group delay shows minimum variation (0.24–0.38 ns) in the passband indicating good linearity. The variations in simulated and measured data are possibly due to loss in two SMA connectors and finite substrate size. The discrepancy in IL can be attributed to the human error involved in fabrication which might have increased/decreased the thickness of conductor/slot lines during the etching process. This in turn would have varied the impedances of  $Z_{0(\text{microstrip})}$  and  $Z_{0(\text{CPW1})}$ , thereby not satisfying the necessary condition of  $Z_{0(\text{microstrip})} = 2Z_{0(\text{CPW1})}$  [6]. The data measured are in reasonable agreement with the simulated response and also accords with the FCC-defined UWB mask for indoor wireless communication. The designed filter is less than one guided wavelength at central UWB frequency (6.85 GHz) which depicts its miniaturized architecture.

The proposed structure is compared with other dual-notched UWB filters in Table 2. It can be observed from the last column

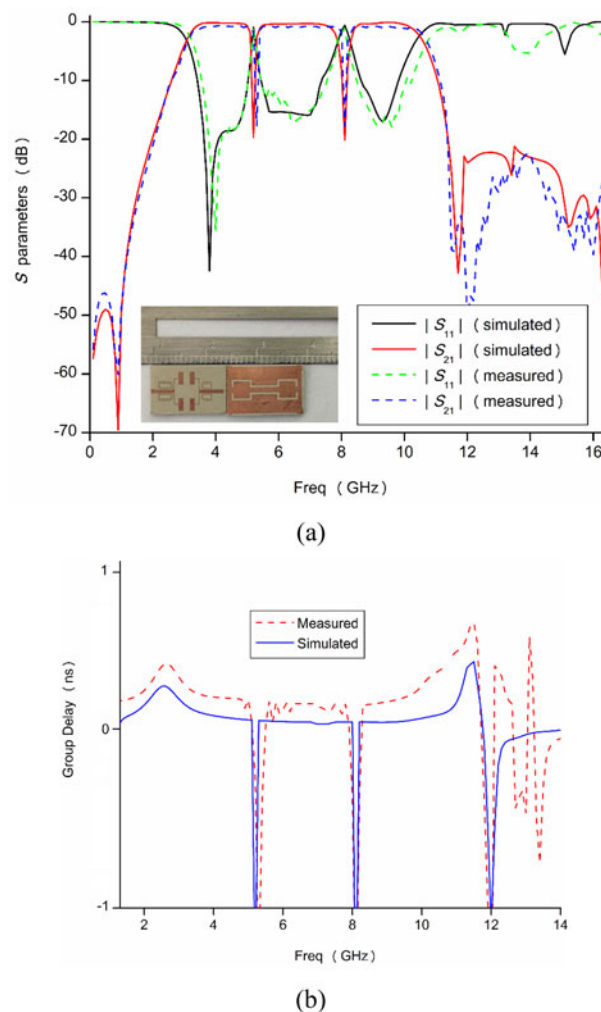


Fig. 8. Comparative BPF frequency responses: (a)  $S$  parameters and (b) group delay.

**Table 2.** Comparison of the proposed band notched filter with other known dual notched structures.

Ref.	Passband (GHz)	IL (dB)	TZs at $f_L$ and $f_H$	Notches (GHz)/attenuation (dB)	Stopband (GHz)/attenuation (dB)	Size ( $\lambda_g \times \lambda_g$ ) at 6.85 GHz
[8]	2.5–12.2	<0.85	X, X	5.15, 7.12/>18	18/>20	1.45 × 0.85
[9]	–	NA	✓, X	5.3, 5.775/>17	20/>15	>0.66 × 0.53
[10]	3.1–10.6	<0.5	✓, ✓	5.2, 5.8/>15	16/>15	>0.88 × 0.71
[11]	2.97–11.2	<0.8	X, X	5.8, 8.1/>20	20/>20	1.31 × 0.45
[12]	2.82–9.64	<1	X, X	6.3, 8/>14	13.2/>18	>1.42 × 1.18
[13]	3.1–10.7	NA	X, X	5.9, 8/>14	20/>10	>0.87 × 0.38
[14]	3.1–10.9	NA	X, X	5.8, 8.7/>14	16/>15	1.2 × 0.95
[15]	3.2–10.9	NA	X, X	5.9, 8/>17	14/>25	0.92 × 0.45
[16]	3.1–10.8	NA	X, X	5.2, 5.8/>14	13/>18	1.36 × 0.85
[17]	2.8–11	<0.8	X, ✓	4.3, 8/>18	14/>15	1.1 × 0.2
[18]	2.8–11	<2	X, X	5.3, 7.8/>17	30/>15	1.01 × 0.5
[19]	3–10.9	<0.6	X, X	5.96, 8.15/>15	16/>20	0.88 × 0.44
[20]	2.6–10.6	<0.8	X, X	3.5, 7.5/>25	12/>28	>1.22 × 0.8
[21]	2.75–10.7	<1.8	✓, ✓	6.1, 8.1/>15.5	18/>15	0.99 × 0.73
This study	3.06–10.73	<1.4	✓, ✓	5.28, 8/>19	16/>23	0.89 × 0.56

Ref., references; IL, insertion loss in the passband (excluding the notches); TZs at  $f_L$  and  $f_H$ , TZs at lower and upper passband edges.

of the table that the proposed structure is compact compared to other studies [8, 10, 11, 12, 14, 16, 18, 20, 21]. The proposed structure possesses TZs at both passband edges unlike most [8, 11–16, 18–20], whereas, others [9, 10, 17] possess TZs at either of the passband edges. This lack of TZs causes their frequency characteristics to degrade. Most of the structures reported have complex geometry due to the presence of vias [11–16, 18, 20] or limitation in fabrication caused by minimum dimension [10, 17]. Our proposed BPF is simple to design due to the absence of vias and limitation of minimum dimension.

## Conclusion

The paper proposes a miniaturized dual-notched UWB filter based on the microstrip-to-CPW transition technology. The short-circuited MMR in ground is excited to equally space its resonant modes within the UWB passband and the coupling of microstrip-to-CPW transition is optimized to generate UWB response with good frequency characteristics. The presence of dual TZs at the passband edges improves the filter selectivity whereas a third TZ provides a spurious free stopband. As such, an UWB-BPF with good frequency characteristics having improved insertion loss/return loss (<0.26 dB/>15 dB) and linear group delay is achieved. Later multiple FSRs are embedded into the BPF to deploy dual passband TZs so as to circumvent possible interferences. The proposed structure being a complete package of compactness and good frequency characteristics calls for its effectiveness in application to modern era UWB communication systems.

## References

1. Revision of Part 15 of the Commission's Rules Regarding Ultra-Wideband Transmission Systems. First Note and Order Federal Communications Commission, ET-Docket (2002), 98–153.
2. Saito A, Harada H and Nishikata A (2003) Development of bandpass filter for ultra wideband (UWB) communication. *Proceedings of IEEE Conference on Ultra Wideband Systems and Technologies*, pp. 76–80.
3. Tang CW and Chen MG (2007) A microstrip ultra-wideband bandpass filter with cascaded broadband bandpass and bandstop filters. *IEEE Transactions on Microwave Theory and Techniques* 55, 2412–2418.
4. Gao J, Zhu L, Menzel W and Bogelsack F (2006) Short-circuited CPW multiple-mode resonator for ultra-wideband (UWB) bandpass filter. *IEEE Microwave and Wireless Components Letters* 16, 104–106.
5. Sahu B, Singh S, Meshram MK and Singh SP (2018) Super-compact ultra-wideband microstrip band-pass filter with improved performance using defected ground structure-based low-pass filter. *Journal of Electromagnetic Waves and Applications* 32, 635–650.
6. Baik JW, Lee TH and Kim YS (2007) UWB bandpass filter using microstrip-to-CPW transition with broadband balun. *IEEE Microwave and Wireless Components Letters* 17, 846–848.
7. Bakali H, Zakriti A, Farkhsi A, Mchbal A and Ouahabi M (2019) Design of a compact UWB BPF using a hybrid structure and a staircase-shaped DGS. *International Journal of Microwave and Optical Technology* 14, 306–313.
8. Ghazali A and Singh A (2016) Band notched UWB-BPF based on broadside coupled microstrip/CPW transition. *IETE Journal of Research* 62, 686–693.
9. Chu QX and Huang JQ (2010) Compact ultra-wideband filter with dual notched bands based on complementary split ring resonators. *Microwave and Optical Technology Letters* 52, 2509–2512.
10. Wu HW and Chen YF (2012) New compact ultra wideband bandpass filter using modified multi-mode resonator. *AEÜ - International Journal of Electronics and Communications* 66, 1021–1025.
11. Nouri S, Nourinia J, Ghobadi C, Alizadeh F and Mohammadi B (2016) Design and analysis of compact BPF with dual notch bands based on stepped-impedance resonator for UWB applications. *Microwave and Optical Technology Letters* 59, 672–674.
12. Gandamalla M, Marathe D and Kulat K (2018) Design and analysis of compact single and dual notch ultra wideband bandpass filter. *Progress in Electromagnetics Research M* 75, 91–102.
13. Wei F, Chen L, Wang ZD and Shi XW (2013) Ultra-wideband band-pass filter with dual narrow notched bands based on dual-mode stepped impedance resonator. *Microwave and Optical Technology Letters* 55, 727–730.
14. Liu BW, Yin YZ, Sun AF, Fan ST and Ren XS (2012) Design of compact UWB bandpass filter with dual notched bands using

novel SCRLH resonator. *Microwave and Optical Technology Letters* **54**, 1506–1508.

15. **Zhao J, Wang J, Zhang G and Li JL** (2013) Compact microstrip UWB bandpass filter with dual notched bands using E-shaped resonator. *IEEE Microwave and Wireless Components Letters* **23**, 638–640.
16. **Liu BW, Yin YZ, Yang Y, Jing SH and Sun AF** (2011) Compact UWB bandpass filter with two notched bands based on electromagnetic bandgap structures. *Electronics Letters* **47**, 757–758.
17. **Song K and Xue Q** (2010) Compact ultra-wideband (UWB) bandpass filters with multiple notched bands. *IEEE Microwave and Wireless Components Letters* **20**, 447–449.
18. **Song Y, Yang GM and Geyi W** (2014) Compact UWB bandpass filter With dual notched bands using defected ground structures. *IEEE Microwave and Wireless Components Letters* **24**, 230–232.
19. **Ghazali AN, Sazid M and Pal S** (2018) A dual notched band UWB-BPF based on microstrip-to-short circuited CPW transition. *International Journal of Microwave and Wireless Technologies* **10**, 794–800.
20. **Zheng X, Pan Y and Jiang T** (2018) UWB bandpass filter with dual notched bands using T-shaped resonator and L-shaped defected microstrip structure. *Micromachines* **9**, 1–11.
21. **Ghazali AN, Sazid M and Pal S** (2020) A miniaturized low-cost microstrip-to-coplanar waveguide transition-based ultra-wideband bandpass filter with multiple transmission zeros. *Microwave and Optical Technology Letters* **62**, 3662–3667.
22. **Psychogiou D, Gomez-Garcia R and Peroulis D** (2018) Wide-passband filters with in-band tunable notches for agile multi-interference suppression in broad-band antenna systems. *2018 IEEE Radio Wireless Symp., Anaheim, CA, USA*, January 14–17, pp. 213–216.
23. **Psychogiou D, Gomez-Garcia R and Peroulis D** (2018) RF wide-band bandpass filter with dynamic in-band multi-interference suppression capability. *IEEE Transactions on Circuits and Systems II: Express Briefs* **65**, 898–902.



**Abu Nasar Ghazali** received his B.Tech. degree in Electronics & Communication Engineering (ECE) from SRM University, Chennai, in 2008 and his M.E. degree in Microwave Engineering from the Birla Institute of Technology (BIT) Mesra, in 2010 where he was a GATE scholar. He completed his doctorate in 2014 from BIT Mesra. He worked as an Assistant Professor in the Department of ECE at the Manav Rachna College of Engineering, Haryana, in 2010 and worked as an Assistant Professor at the BIT Mesra, Patna campus. Currently, he is an Assistant Professor (II) in the School of Electronics Engineering, at the Kalinga Institute of Industrial Technology (KiiT), Deemed University, Bhubaneswar, India. He is an Associate member, The Institution of Engineers (IEI), India, and member of IEEE. He has published quite a few papers in peer reviewed journals and conferences. His main research interests are UWB filters, UWB antennas, defected ground structures, microstrip filters, and microwave circuit components.



**Mohammad Sazid** received his B.Tech. degree in Electronics & Communication Engineering (ECE) from Uttar Pradesh Technical University in 2011 and his M.E. degree in Wireless Communication Engineering from BIT Mesra, in 2015 where he was a GATE scholar. He is currently working as an Assistant Professor in the Department of ECE at the Noida Institute of Engineering & Technology. He is also pursuing his doctorate from the Delhi Technological University (DTU), New Delhi. He has published several papers in SCI journals. His main research interests are UWB filters and passive microwave circuit components.